

Low Space-Charge Intensity Beams in UMER via Collimation and Solenoid Focusing

S. Bernal¹, B. Beaudoin¹, L. Dovlatyan¹, S. Ehrenstein², I. Haber¹, R. A. Kishek¹,
E. Montgomery¹ and D. Sutter¹

¹*Institute for Research in Electronics and Applied Physics, University of Maryland, College Park, MD 20742*

²*Case Western Reserve University, Cleveland, OH 44106*

^{a)}Corresponding author: sabern@umd.edu

Abstract. The University of Maryland Electron Ring (UMER) has operated traditionally in the regime of strong space-charge dominated beam transport, but small-current beams are desirable to significantly reduce the direct (incoherent) space-charge tune shift as well as the tune depression. This regime is of interest to model space-charge effects in large proton and ion rings similar to those used in nuclear physics and spallation neutron sources, and also for nonlinear dynamics studies of lattices inspired on the Integrable Optics Test Accelerator (IOTA). We review the definition of space-charge intensity, show a comparison of space-charge parameters in UMER and other machines, and discuss a simple method involving double collimation and solenoid focusing for varying the space-charge intensity of the beam injected into UMER.

INTRODUCTION

The initial motivation of the University of Maryland Electron Ring (UMER) [1] has been expanded recently to include nonlinear dynamics studies in lattices inspired on the Integrable Optics Test Accelerator (IOTA) at Fermilab [2], but space-charge (SC) effects must be reduced significantly to conduct “zero” beam-current control experiments [3]. Furthermore, SC effects are increasingly important for new and upgraded large storage and accumulator proton and ion rings, but some of these are user facilities with limited time for beam physics experiments. Examples of these machines are the Spallation Neutron Source (SNS) at Oak Ridge national Laboratory, and the heavy-ion synchrotrons (“SchwerIonenSynchrotron”) SIS-18, and SIS-100 in Germany. The tune shift from small (relative to the horizontal bare tune ν_{0x}) direct (incoherent) SC effects is given by [4]

$$\Delta\nu_x = \nu_{0x} - \nu_x = \frac{r_{e,p}}{\pi} \frac{N}{\beta^2 \gamma^3} \left[\epsilon_x \left(1 + \sqrt{\frac{\epsilon_y \nu_{0x}}{\epsilon_x \nu_{0y}}} \right) \right]^{-1} \left(\frac{q_s^2}{A} \right) \left(\frac{F_x G_x}{B_f} \right), \quad (1)$$

where the first factor contains the classical radius of the electron or proton, the second one the number of particles per bunch N and the relativity-theory parameters β and γ , and the third one the un-normalized, rms emittance terms. The last two factors include the charge state q_s , the mass number A , and parameters related to image forces (F_x), type of distribution (G_x), and bunching factor (B_f). Over a broad range of energies and beam currents in machines in operation, the tune shift is $\Delta\nu_x = 0.1 - 0.5$. In UMER, typically $\Delta\nu_x = 1.0 - 5.0$.

Further, “beam intensity” is loosely defined as proportional to N , with “space-charge limited” meaning $\Delta\nu$ less than 0.5 (Laslett criterion [5]). However, “SC intensity,” χ , as introduced independently by Reiser and Davidson, is related to $\Delta\nu/\nu_o$, not just to N or $\Delta\nu$ [6]. For small SC effects [7],

$$\chi \simeq \frac{2\Delta\nu}{\nu_0} = \frac{KR_m}{\epsilon\nu_0}, \quad K = \frac{I}{I_{0e,p}} \frac{2}{\beta^3 \gamma^3}. \quad (2)$$

In equation (2), K is the beam perveance or SC parameter [6], R_m the machine average radius, and $I_{0e,p}$ is a characteristic current equal, approximately, to 17 kA for electrons, and 31 MA for protons. For ions the characteristic current is $31MA \times A$, approximately, where A is the mass number. For the sake of simplicity, we have omitted the

subscript “ x ” in the tune in equation (2). Note also that the ratio R_m/ν_0 is the single-particle average betatron function. Although increasing the operating tune would be an obvious way to reduce SC intensity in UMER, the reduction would not be substantial, because the tune would be limited to a maximum of around 8.9 (standard ν_0 is around 6.6.) Moreover, practical problems would arise with overheating of the quadrupole magnets.

Another effect that arises from image forces and SC leads to a *coherent* tune shift. This effect is ordinarily small at low energies compared to the incoherent tune shift because it is proportional to the ratio $(a_0/h)^2$, where a_0 , h are the zero-current average radius, and the half-gap of the vacuum pipe, respectively [7].

The *tune depression*, which is more commonly used than χ , is given by $\nu/\nu_0 = (1 - \chi)^{1/2}$, for arbitrary but linear SC. Because of UMER’s low energy (10 keV), K is large even for the smallest beam currents, which compensates for the small machine radius to yield significant SC intensities. *Both* the tune shift and the SC intensity χ are important for characterizing beam dynamics: the former is naturally relevant to betatron resonance crossing, while the latter can be related to transverse beam stability in general [6]. Despite obvious differences in injection methods, beam loss mechanisms, and bunch structure, UMER and the larger, planned or upgraded, high-energy ion rings share key features: significant SC effects, the absence of synchrotron radiation, and a modest number of turns (100-1000). However, we must reduce the ratio K/ϵ significantly in UMER to approach the tune shifts and SC intensities of the larger machines.

SPACE CHARGE IN UMER AND OTHER MACHINES

Table 1 summarizes parameters and SC calculations for 4 cases of UMER operation, 3 cases of large, high-energy rings, and the IOTA proton ring at Fermilab. The standard operation at 10 keV, 6 mA (nominal) in UMER ($\nu_{0x} = 6.6$) yields SC numbers close to the corresponding ones for a possible heavy-ion fusion (HIF) driver [8]. Operation at 10 keV, 40 μA using the DC electron gun method described in [9] yields a beam with negligible SC parameters, as in a light source. Operation at 10 keV, 50 μA (see last section), would correspond roughly to the SC regime of the proton accumulator ring at the Spallation Neutron Source (SNS) at Oak Ridge National Laboratory at the end of the accumulation cycle (1,000 turns). At the lowest end of SC in UMER standard operation, we obtain SC parameters as in the IOTA proton ring. The operation of UMER with lower beam currents produced by double collimation and solenoid focusing is described later.

TABLE 1. Parameters relevant to direct space-charge in electron and ion rings

Machine, Circumference	Kinetic Energy, $\beta = v/c$	Peak Current, RMS Emittance (norm.)	ν/ν_0 , $\Delta\nu$
UMER, 11.52 m	10 keV, 0.195	6.0 mA, 1.3 μm^*	0.63, 2.4
HIF Xe^{+8} Driver, 429 m	10 GeV, 0.381	1.0 kA, 50 m	0.66, 2.1
UMER, 11.52 m	10 keV, 0.195	40 μA , 5.0 μm^\dagger	1.00, 0.005
ALS (LBNL), 197 m	1.2 GeV, 1.000	400 mA, 3.5 nm	1.00, 0.00
UMER, 11.52 m	10 keV, 0.195	50 μA , 0.07 μm^\ddagger	0.93, 0.45
SNS Acc. Ring, 248 m	1.0 GeV, 0.875	52 A, 120 m	0.98, 0.15
UMER, 11.52 m	10 keV, 0.195	0.6 mA, 0.4 μm	0.86, 0.94
IOTA Proton Ring, 40 m	2.5 MeV, 0.073	8 mA, 0.3 μm	0.96, 0.5 (1.2) §

*Typical operation.

† DC electron gun operation. See [9].

‡ Double collimation (see Table 3).

§ Unbunched (bunched) See [2].

Another important aspect of beam dynamics that justifies operation with low SC-intensity beams in UMER is beam debunching. Without longitudinal containment, coasting beams in UMER, initially filling half the ring circumference, elongate until the two bunch ends meet after a number of turns. A one-dimensional fluid model allows us to calculate the “sound” speed C_S , i.e., the speed of charge rarefaction, and approximate debunching times according to [7, 10]

$$C_S = \sqrt{\frac{eg\Lambda_0}{4\pi\epsilon_0\gamma^5 m_e}}, \quad \tau = \frac{1}{4C_S} (C - L_b). \quad (3)$$

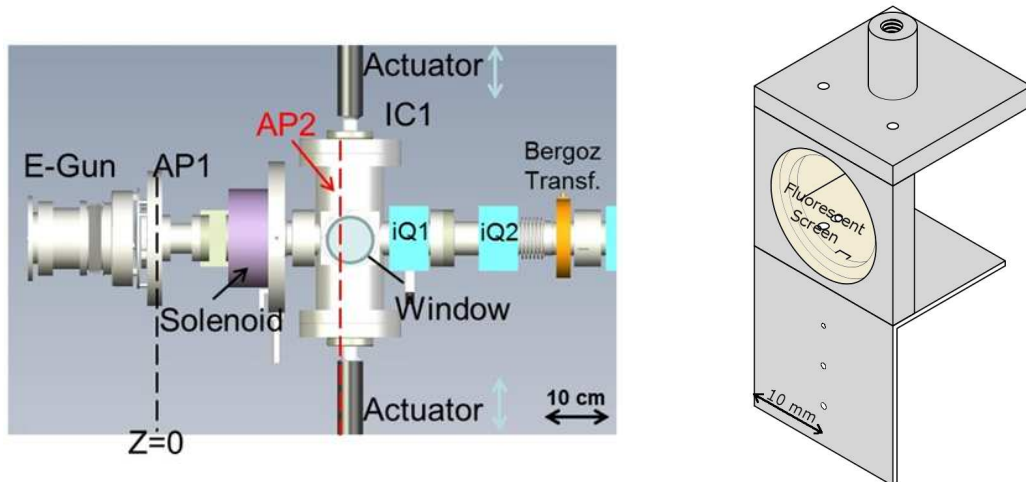


FIGURE 1. Left: Schematics of the first few elements in the straight section of UMER: electron gun, plane of aperture disk (AP1), solenoid lens, diagnostic chamber 1 (IC1) with window, plane of second aperture (AP2), actuators, and first two quadrupole lenses. The top actuator houses fluorescent screen diagnostics and AP2. Right: New aperture plate (AP2) attached to the bottom of the fluorescent-screen cube - 3 small apertures are shown.

The constant $\Lambda_0 = I_b/\beta c$ is the peak longitudinal charge density, and g is a form factor of order unity. C is the machine circumference (11.52 m) and L_b the bunch's length corresponding to 100 ns. Since the leading and trailing tails of the bunch are not well defined, the debunching time as defined above is only a reference parameter. Actually, the space charge waves inside the bunch collapse at a time 2τ [10]; further, beam current is still detected by the resistive wall-current monitor in UMER for times of the order of 4τ . Table 2 summarizes results of longitudinal expansion. With properly applied longitudinal focusing we can extend the number of turns by a factor of 40 for 0.6 mA and 10 for 6 mA.

TABLE 2. Beam debunching in UMER is greatly reduced at low current.

Beam Current	“Sound Speed” C_S (m/s)	Approx. No. Turns To Debunch	Approx. No. Turns With Long. Focusing
$60 \mu A$	10^5	70	
0.6 mA	3×10^5	25	1,000
6.0 mA	8×10^5	9	100
21 mA	10^6	6	
104 mA	2×10^6	3	

Independent control of current and transverse emittance is desirable, but can only be partially realized in practice. We have produced different beam currents with apertures located near the electron gun output. Naturally, the beam current scales with the area of the aperture, while the emittance scales with the aperture radius. However, the smallest SC intensity achieved in this way still leads to an incoherent SC tune shift of almost unity under typical operating tunes in UMER. To achieve lower incoherent SC tune shifts and intensities, ultra-low currents can be obtained with three methods: DC electron-gun operation, photoemission, and double collimation assisted with solenoid focusing. All three methods are discussed briefly in [9]. In the next section we describe in detail measurements and SC calculations related to the third method, which we regard as the simplest one to implement in UMER.

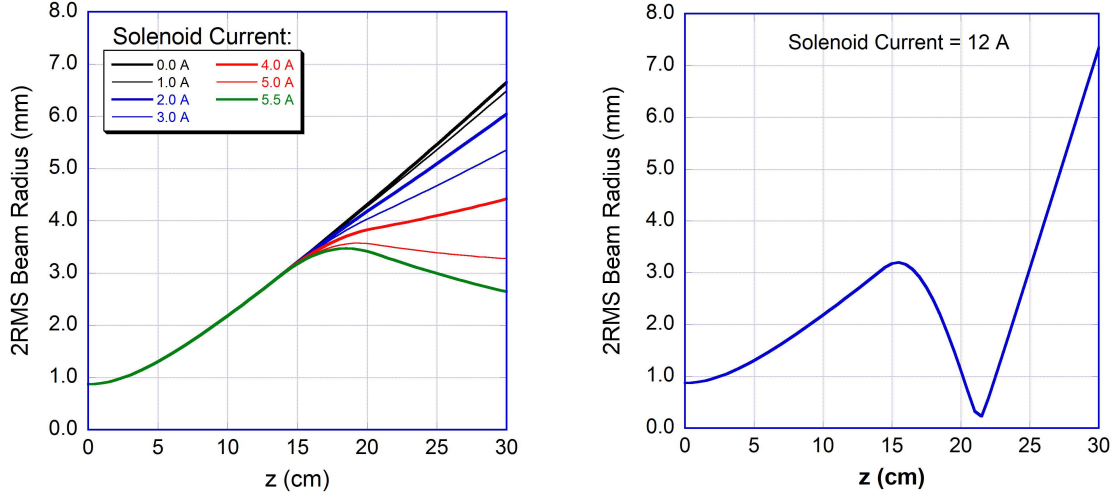


FIGURE 2. Left: evolution of $2\times$ rms beam envelope radius from AP1 to AP2 (see Fig. 1) for 7 values of solenoid current for the 6.0 mA (nominal) beam. Right: evolution of the envelope with solenoid over-focusing. The short solenoid is located at $z = 17.6$ cm from AP1.

LOW SPACE-CHARGE INTENSITY BY DOUBLE COLLIMATION AND SOLENOID FOCUSING

Figure 1, left, shows the schematics of the first few elements downstream of the electron gun in UMER. We employ two sets of apertures, AP1 and AP2, and solenoid focusing. As shown in Figure 1, right, the cube that houses fluorescent screen diagnostics in IC1 is fitted at the bottom with a plate containing 3 apertures of varying radii. After viewing the beam and then adjusting its size with solenoid focusing, it is possible to accurately position one of the apertures to obtain small beam currents. The plot in Figure 2, left, illustrates the calculated envelope of the 6 mA (nominal) beam over 30 cm from AP1 to AP2 for seven values of solenoid current. It is possible to over-focus the beam to yield even larger beams onto AP2 than with zero solenoid current. Figure 2, right, displays the beam envelope from AP1 to AP2 when the solenoid current is 12 A.

The 6 mA beam expands freely (solenoid current = 0 A) from a radius of 0.875 mm at AP1 to 6.7 mm at AP2. Thus, a second aperture AP2 of radius 0.67 mm yields a new current of $50 \mu\text{A}$ past AP2, with an estimated rms normalized emittance equal to $0.073 \mu\text{m}$. The emittance of the apertured beam is obtained from simulations with the WARP code [12]; it can be estimated also by simply multiplying the experimental 6 mA emittance ($0.75 \mu\text{m}$) by $(0.67/6.7)$. The experimental emittance of the $50 \mu\text{A}$ beam, however, is smaller, $0.05 \mu\text{m}$. It is obtained via a standard quadrupole scan whereby the $2\times$ rms beam radii squared (at a screen 40 cm downstream from AP2) are plotted as a function of quadrupole ($iQ1$) current; the emittance is extracted from the parabolic fit constants.

Changing solenoid focusing to vary the beam radius at AP2 yields varying SC intensities for beam transport in UMER (SC intensity as defined for a matched beam in a periodic lattice - see equation (2), and the more general formula in [7].) Figure 3, left, shows results of beam radius at AP2 from experiment, solutions of the K-V envelope equations [6, 7], and WARP simulations, as a function of solenoid current. The WARP simulations employ an initial semi-Gaussian distribution at AP1, 40,000 macro-particles and a solenoid field that includes terms to fifth order. There is very good agreement between calculations and experiment for solenoid currents from 0 to 7 A, and between WARP simulations and envelope calculations for all solenoid currents.

The variation in SC intensity is illustrated in Figure 3, right, where both the incoherent SC tune shift (left axis) and the tune depression (right axis) are plotted as a function of solenoid current. The operating tune in UMER for these calculations is $\nu_0 = 6.6$. The effective emittances past AP2 are extracted from WARP simulations, while the beam currents are the initial beam current scaled by the ratio $(0.67 \text{ mm}/\text{beam radius at upstream plane of AP2 (mm)})^2$. Only one point in Fig. 3, right, at solenoid current of 7 A, corresponds to SC-dominated beam transport for which the tune depression is < 0.71 ; the point at 8 A is borderline between SC- and emittance-dominated transport. At a solenoid

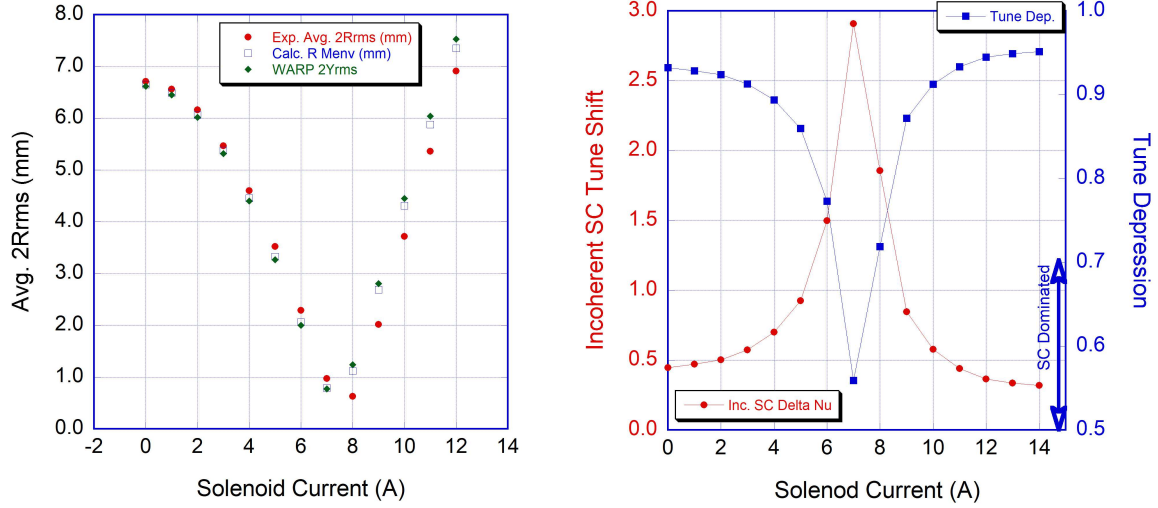


FIGURE 3. Left: Beam radius at upstream plane of aperture AP2 as a function of solenoid current (see Fig. 1); results from experiment, envelope calculations and simulations with the WARP code are shown. Right: Direct space charge parameters, tune shift (left axis) and tune depression (right axis). The arrow on the tune depression scale indicates the region of SC dominated transport (only one point is clearly in that region - see also table 3.)

current of 7 A, the effective beam radius at AP2 is close to 1 mm (Fig. 3, left), leading to a beam current of near 3 mA past AP2 and an emittance smaller but close to the original one for the 6 mA beam. Note also that over-focusing the beam (solenoid current > 10 A) leads to slightly smaller SC tune shifts, and tune depressions closer to 1.0. Table 3 summarizes the cases discussed so far and includes the dimensionless SC intensity parameter χ , which is < 0.5 for emittance-dominated transport. The table also contains partial experimental data of beam current and emittance; we are working on solving alignment issues with the solenoid to extend the measurements.

Figure 4 shows pseudo-color versions of fluorescent screen beam pictures at AP2 for three cases of solenoid current: 7 A, 6 A, and 10 A (see also Fig. 3). The WARP simulations do not reproduce the halos seen at 6 and 7 A, indicating that their source, if real, is not from solenoid spherical aberration, which is included in the solenoid model. However, the relative intensities and shapes of the halos lead us to believe that only the halo for the 6 A case is real: the large halo is as dim as the round ghost images (about 1 – 2 out of 255 for 8-bit grayscale pictures) and perfectly formed. The actual halo would be blocked by the bottom aperture at AP2 (radius = 0.67 mm), but it could reappear downstream leading to an rms emittance significantly larger than calculated at a solenoid current of 6 A.

In conclusion, double collimation and solenoid focusing can be used to vary the SC intensity and reduce the incoherent tune shift from 2 - 3 to < 0.5, and change the tune depression from 0.55 to > 0.9. Naturally, using the middle and top apertures at AP2 (Fig. 1, right), which are smaller than the one used for calculations and measurements for this work, could lead to additional reduction of direct SC, but S/N issues arise because of the small currents thus obtained.

TABLE 3. Effect of solenoid focusing on beam and space-charge parameters with 6 mA at AP1, and AP2 radius = 0.67 mm. The operating tune in UMER is $\nu_0 = 6.6$.

Solenoid Current	Beam Current, RMS Emittance (norm.)	SC Intensity	
		$\nu/\nu_0, \Delta\nu$	χ
0 A	49.6 (58)* μA , 0.073 (0.05)* μm	0.93, 0.45	0.130
2	60.0 (63)* μA , 0.078	0.92, 0.50	0.146
4	112 (99)* μA , 0.103	0.89, 0.70	0.201
7	3.70 mA, 0.615	0.56, 2.91	0.687
8	1.41 mA, 0.434	0.72, 1.86	0.483
12	68.6 μA , 0.070	0.94, 0.36	0.107

*Measured (in parenthesis).

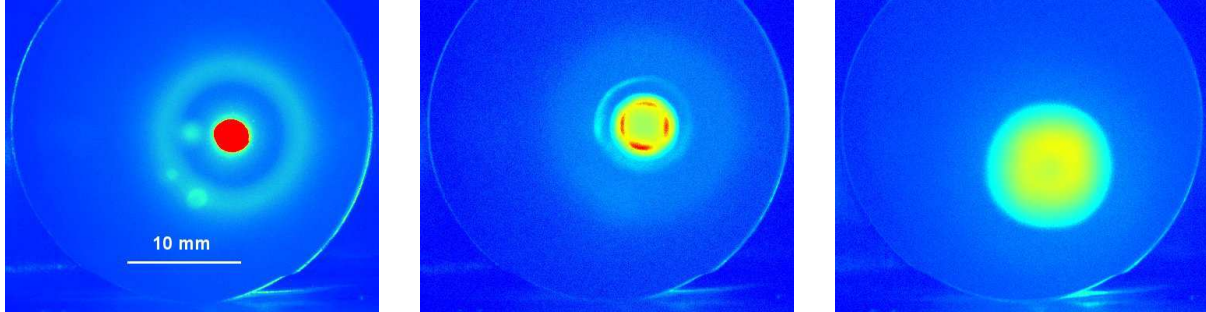


FIGURE 4. Pseudo-color renderings of fluorescent screen beam pictures at upstream plane of AP2 (see Fig. 1, right) for a solenoid current of 7 A (left), 6 A (middle), and 10 A (right). Both the halo and ghost images for the 7 A case (left) are from the camera optics and/or fluorescent screen; the halo for the 6 A case is deemed real.

ACKNOWLEDGMENTS

This work was supported by the Office of Science, Office of High Energy Physics of the U.S. Department of Energy.

REFERENCES

- [1] R. A. Kishek et al., Nucl. Instrum. Meth. Phys. Res. A 733, 233237 (2014).
- [2] S. Antipov et al., IOTA (Integrable Optics Test Accelerator): facility and experimental beam physics program, Journal of Instrumentation, Volume 12, March 2017.
- [3] K. Ruisard, H. Baumgartner, B. Beaudoin, I. Haber, D. Matthew, and T. Koeth, Proceedings of NAPAC2016, Chicago, IL, p. 507.
- [4] K. Schindl, Space Charge, in CERN Accelerator School 2003: Intermediate Course on Accelerators, CERN-2006-002 (2006).
- [5] L. J. Laslett, On intensity limitations imposed by space charge effects in circular particle accelerators, in Proceedings of the 1963 Summer Study on Storage Rings, Brookhaven Nat. Lab., Report BNL 7354 (1963), p. 324.
- [6] M. Reiser, Theory and Design of Charged Particle Beams, 2nd Ed., Wiley-VCH (2008).
- [7] S. Bernal, A Practical Introduction to Beam Physics and Particle Accelerators, Morgan & Claypool Pub., IOP Concise Physics (2016).
- [8] J. J. Barnard et al., Recirculating induction accelerators as drivers for heavy ion fusion, Phys. Fluids B 5, 2698 (1993).
- [9] S. Bernal et al., Ultra-low current beams in UMER to model space-charge effects in high-energy proton and ion Machines, Proceedings of the 17th Advanced Accelerator Concepts Workshop (AAC 2016), National Harbor, MD.
- [10] D. F. Sutter and B. L. Beaudoin, Measurement of plasma wave speed from electron beam end erosion, Proceedings of PAC2013, Pasadena, CA, p. 520.
- [11] S. Bernal, B. Beaudoin, M. Cornacchia, and D. Sutter, Stability of Emittance vs. Space-Charge Dominated Beams in an Electron Recirculator, Proceedings of PAC2013, Pasadena, CA, p. 514.
- [12] A. Friedman, R. H. Cohen, D. P. Grote, S. M. Lund, W. M. Sharp, J.-L. Vay, Irving Haber, and R. A. Kishek, Computational methods in the warp code framework for kinetic simulations of particle beams and plasmas, IEEE Trans. Plasma Sci. 42(5), 1321 (2014).